

Validation of Methods for Estimation of Knee Joint Mechanical Impedance During Locomotion Using a Torque-Controllable Knee Exoskeleton

Yves F. Nazon II

Department of Mechanical Engineering,
Robotics Institute University of Michigan,
Ann Arbor, MI 48109
e-mail: nazon@umich.edu

Raveena M. Doshi

Department of Mechanical Engineering,
Robotics Institute University of Michigan,
Ann Arbor, MI 48109
e-mail: rmdoshi@umich.edu

Elliott J. Rouse

Mem. ASME

Department of Mechanical Engineering,
Robotics Institute University of Michigan,
Ann Arbor, MI 48109
e-mail: ejrouse@umich.edu

The mechanical impedance of the joints of the leg governs the body's response to external disturbances, and its regulation is essential for the completion of tasks of daily life. However, it is still unclear how this quantity is regulated at the knee during dynamic tasks. In this work, we introduce a method to estimate the mechanical impedance of spring-mass systems using a torque-controllable exoskeleton with the intention of extending these methods to characterize the mechanical impedance of the human knee during locomotion. We characterize system bandwidth and intrinsic impedance and present a perturbation-based methodology to identify the mechanical impedance of known spring-mass systems. Our approach was able to obtain accurate estimates of stiffness and inertia, with errors under 3% and \sim 13–16%, respectively. This work provides a qualitative and quantitative foundation that will enable accurate estimates of knee joint impedance during locomotion in future works. [DOI: 10.1115/1.4051843]

1 Introduction

Careful regulation of knee joint mechanics is an integral part of successful balance, locomotion, and countless activities of daily life. Knowledge of how these mechanics are regulated is essential to understanding how humans achieve stable gait as muscles spanning the knee provide support to the body and decelerate the limb during stance phase, deliver power to accelerate the trunk [1], and absorb energy during terminal swing phase [2]. These mechanics—collectively known as *joint mechanical impedance*—govern the body's instantaneous response to disturbances and regulate energy storage and exchange during movement [3–5]. Studies have demonstrated that humans are able to regulate joint impedance consciously and subconsciously to adapt to unexpected changes during dynamic tasks [6–8]. A thorough characterization of knee impedance has significant implications for studying and improving locomotion, including insights into human motor control, treatment of neuromotor pathologies, and development of biomimetic assistive technologies.

While knee mechanical impedance has been extensively studied under certain conditions, a holistic understanding of these properties during dynamic tasks is still lacking. The mechanical impedance of the knee has been characterized during postural tasks and shown to vary with joint angle and muscle activation level [3,9,10]. Several studies have demonstrated that joint impedance during dynamic tasks is different from what has been shown for postural tasks [11–13]. While some studies have generated model-based estimates of knee impedance during movement [14–16] or characterized the torque-angle relationship of the knee during gait [17] (which is different from the stiffness of the knee [18]), these results have not yet been compared to data obtained from empirical biomechanical studies.

For a device to be capable of estimating joint mechanical impedance, it must meet three functional requirements: the ability to apply a torque or position perturbation to the joint, the ability to measure the torque applied to the joint during the perturbation,

and the ability to measure the position displacement of the joint during the perturbation. A number of exoskeletons have been designed to perturb the knee during locomotion, and these exoskeletons employ a range of perturbation paradigms [19–22]. These paradigms include flexion/extension locking [19], knee flexion torque assistance [20], and angular positional perturbations [21,22]. However, these exoskeletons cannot provide perturbations bidirectionally, with the exception of Tucker et al. [22]. Furthermore, these devices were developed for different applications (i.e., locomotor assistance) and have not been used to quantify knee mechanical impedance in static or dynamic conditions.

Estimation of joint mechanical impedance from experimental data is typically attained using linear techniques. Linear techniques commonly describe joint impedance in terms of a nonparametric impulse response function or a parameterized second-order system consisting of stiffness, damping, and inertia [3]. Previous works used a parametric approach to characterize the mechanical impedance of the ankle throughout the gait cycle, which employed both linear time varying [23] and linear time invariant methods [4,24]. Lee et al. utilized a wearable ankle device to provide controlled torque perturbations to the ankle directly and quantified how ankle impedance varied during the swing phase of gait [23]. Rouse et al. and Shorter and Rouse took a different approach, leveraging an instrumented walkway to apply kinematic perturbations to the ankle indirectly to obtain impedance parameters during the stance phase of gait [4,24].

The contribution of this paper is validating the novel combination of experimental and analytical methods for estimating knee joint mechanical impedance with a torque-controllable exoskeleton. We propose the use of a torque perturbation paradigm with an untethered, wearable knee exoskeleton that can apply bidirectional torque perturbations. This exoskeleton measures the torque applied to the knee joint and the displacement of the knee joint while a perturbation occurs. We utilize parametric linear time invariant methods to estimate the mechanical impedance of known second order systems, consisting of an external spring and moment of inertia. We demonstrate the efficacy of our methods through characterization of the exoskeleton's torque bandwidth and intrinsic mechanical impedance properties. In addition, we

Manuscript received September 22, 2020; final manuscript received June 17, 2021; published online December 15, 2021. Assoc. Editor: Sara Wilson.

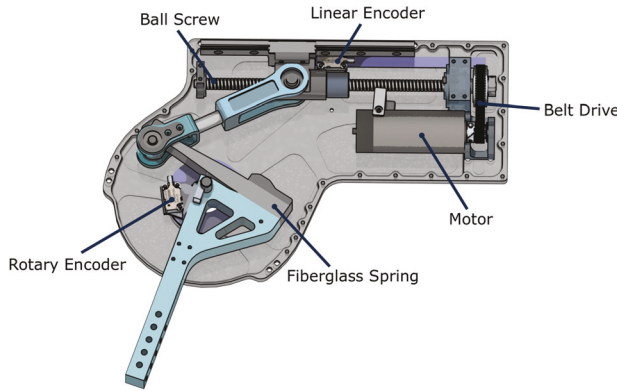


Fig. 1 Diagram of the Neurobionics torque-controllable exoskeleton. The fiberglass spring serves as the series elastic element in the actuator, connecting the transmission to the output shaft.

validate the system identification capabilities of our approach using a three-pronged comparison. First, we compare our results to those independently measured via materials testing protocols. Next, we compare our results to existing state of the art joint impedance measurement devices. Finally, we compare our results to the human body's ability to sense changes in impedance. We use the information from these three comparisons to adjudicate if the combination of our device and methods are valid for estimating knee joint impedance during walking. Validation of our approach will provide a foundation and reference for future studies to characterize the mechanical impedance of the human knee joint during locomotion.

2 Methods

2.1 Torque-Controllable Exoskeleton. To apply a perturbation, we must be able to mechanically interact with the knee joint. To this end, we utilize a torque-controllable exoskeleton developed previously by our group; a full description of the device is found in Shepherd and Rouse [25]. Briefly, a brushless dc motor (EC30, Maxon Motor, Sachseln, Switzerland) drives a 2.5 mm lead ball screw (Thomson Industries, Inc., Radford, VA) after a 2:1 belt drive (Fig. 1). A two force member connects the ballnut to a cantilever fiberglass leaf beam (E-glass, Gordon Composites, Montrose, CO). This fiberglass leaf spring functions as a series elastic element between the transmission and the exoskeleton output, with a translational stiffness of 274 N/mm to a perpendicular load. Two submicron resolution optical encoders (ATOM; Renishaw, Wotton-under-Edge, Gloucestershire, UK) placed before and after the spring in the drivetrain measure the angular deflection of the spring. This angular deflection is used to estimate the applied torque (Fig. 2). Closed loop torque control of the exoskeleton is implemented in Python on a single board computer (model: Raspberry Pi 3 Model B, Raspberry Pi Foundation, Cambridge, UK).

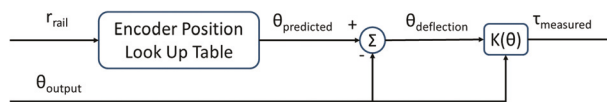


Fig. 2 Block diagram of exoskeleton torque calculation. Deflection of the fiberglass spring is calculated as the difference between the position estimated by the linear encoder and the position measured by the rotary encoder. This deflection is multiplied by the position-dependent stiffness of the fiberglass spring to provide an estimate of the torque applied by the exoskeleton.

2.2 Characterization of Exoskeleton Bandwidth and Intrinsic Impedance. We characterized the system's torque bandwidth to understand the available frequency content of torque perturbations. To determine system bandwidth, two Gaussian white noise reference signals with amplitudes of 20 and 40 N·m, low-pass filtered using a third-order Butterworth filter with a cut-off frequency of 40 Hz, were provided as reference inputs for the exoskeleton torque controller. We measured the output torque (τ) and then estimated the system's frequency response from the input and output data using Blackman-Tukey spectral analysis with a 500 sample Hann window in MATLAB (MathWorks, Natick, MA). We determined bandwidth by locating the frequency at which the magnitude dropped below -3 dB.

To characterize the intrinsic mechanical impedance of the device (i.e., its own internal inertial (J), viscous (B), and elastic (K) characteristics), a Gaussian white noise signal was used as the reference input for closed-loop position control. The white noise signal was low-pass filtered using a third-order Butterworth filter with a cutoff frequency of 20 Hz. The filtered signal was provided for three 10-second trials, during which actuator output position ($\theta(t)$) and measured torque (τ) were collected at a sample rate of 1 kHz. Following data collection, an interior point optimization method was used to resolve impedance estimates in MATLAB. Final estimates were determined by selecting values that minimized the mean squared error of the estimated and measured torque signals, where estimated torque is defined by the relationship in Eq. (1)

$$\tau(t) = J\ddot{\theta}(t) + B\dot{\theta}(t) + k\theta(t) \quad (1)$$

Following estimation of the parameters in Eq. (1), variance accounted for (VAF) was used to compare the torque estimated from the parameters to the measured response. VAF indicates how adequately a model output predicts the variance of measured data and is defined by Eq. (2) where $\tau_{\text{est}}(t)$ is the estimated torque calculated from the impedance parameters as a function of time and $\tau_{\text{meas}}(t)$ is the torque measured from the exoskeleton

$$\text{VAF} = \left[1 - \frac{\sum \tau_{\text{est}}(t) - \tau_{\text{meas}}(t)^2}{\sum \tau_{\text{meas}}(t)^2} \right] * 100 \quad (2)$$

2.3 Computation of External Inertia and Spring Stiffness Values. The tested inertias, I_1 and I_2 , consisted of a top and bottom bar constructed from 6061 aluminum and an interchangeable center bar constructed from 6061 aluminum or 1018 low carbon steel. Moments of inertia were determined by measuring the dimensions of the top, bottom, and center bars as well as the centroid distance of each bar from the axis of rotation, and the mass of each component (Fig. 3). With this information, the closed form solution of moment of inertia was used to calculate the values of I_1 and I_2 . Spring stiffness was experimentally determined by measuring the deflection of two linear springs (McMaster-Carr, Elmhurst, IL), k_1 and k_2 , in their linear region of operation. Two different weights (W_1 , W_2) were applied to the spring, and the elongated position of spring was measured. The magnitude of each weight was determined by recording measurements from a force plate for one second, sampled at 1000 Hz (Bertec Corporation, Columbus OH). Spring elongation was measured using a motion capture system, sampled at 100 Hz for five seconds (Vicon Motion Systems Ltd., Oxford, UK). The process to determine spring stiffness was as follows: springs were loaded, the elongation was measured, and then, the spring was unloaded. This process occurred three times for each spring at each weight level.

2.4 Dynamic Estimation of Mechanical Impedance. We validated new methods for estimating mechanical impedance by interacting with known mechanical systems and comparing our estimated values with those independently measured. We matched

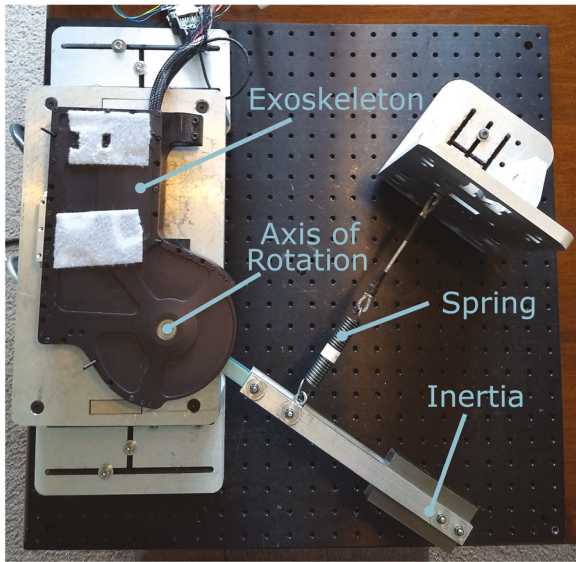


Fig. 3 Diagram of the experimental setup. Labeled components are the actuator and its axis of rotation, the spring and the inertia.

two masses with known moments of inertia (I_1, I_2) to two springs (k_1, k_2) to test four spring-inertia combinations. We chose inertia values that correspond to one half (I_1) and one (I_2) times the inertia of the human shank and foot [26]. We chose spring stiffness values that span the range of human knee stiffness values in literature [9]. The spring-inertia combinations tested are denoted as cases 1–4 hereafter, where case 1 is k_1 matched with the I_1 , case 2 is k_2 matched with I_1 , case 3 is k_1 matched with I_2 , and case 4 is k_2 matched with I_2 . During benchtop tests, the tested inertia was rigidly attached to the output shaft, and the tested spring was suspended between the output shaft and a fixed testing jig (Fig. 3). The viscous (i.e., damping) component of the system was not externally imposed and instead includes only the viscous loss incurred after the elastic element within the exoskeleton, bearing friction, and other minor sources of velocity-dependent loss.

When a perturbation is applied during walking, the torques and angles that result from the motion must be removed to enable analysis of the perturbation response alone. To experimentally replicate this scenario, a sinusoidal torque was prescribed to the exoskeleton, upon which torque perturbations were superimposed. Each case was matched to five underlying torque trajectories, ψ_{A-E} , described in Eqs. (3)–(7). Each sine wave had the form $A \sin(\omega t) + B$ where A is the amplitude in Nm, ω is the frequency

in Hz, t is the time in seconds, and B is the torque offset in Nm. The tested frequencies were chosen to encompass the known frequency of able-bodied human walking [27], previous dynamic impedance experiments [24,28], and the frequency of pathological gait [29,30]. To ease descriptions of the case-trajectory combinations, they are referred to hereafter by the spring inertia combination (case numbers: 1–4) followed by the trajectory type (A–E) (1 A, 3D, etc.):

$$\psi_A = 5 \sin(1.4t) + 32 \quad (3)$$

$$\psi_B = 5 \sin(0.8t) + 32 \quad (4)$$

$$\psi_C = 5 \sin(2.0t) + 32 \quad (5)$$

$$\psi_D = 6 \sin(1.4t) + 32 \quad (6)$$

$$\psi_E = \frac{1}{2}[5\sin(1.4t) + 6\sin(2.0t) + 40] \quad (7)$$

The perturbations superimposed on these underlying trajectories all had a magnitude of seven Nm and consisted of a ramp of 75 ms, a 100 ms hold, and a negative 75 ms ramp. The onset of these perturbations was at 10%, 40%, 60%, or 90% of the sine wave corresponding to the middle of the loading phase, midterminal stance, toe-off, and the transition from mid to terminal swing phase of the gait cycle, respectively.

Perturbation extraction resulted from the subtraction of two trajectories. The initial trajectory was a sinusoidal trajectory of the form of ψ_{A-E} . The following trajectory was the same initial trajectory (ψ_{A-E}) with perturbations overlaid on the initial trajectory. By subtracting the initial trajectory from the following trajectory, perturbation isolation was achieved (Fig. 4). This isolation process occurred for both the output torque and output position measured by the exoskeleton. Following extraction, the bootstrapping technique from Rouse et al. was used to estimate variability of the isolated perturbations [31]. The bootstrapped perturbations were segmented and analyzed in a 100-ms window following the onset of the perturbation. The segmented position perturbations were twice differentiated to obtain velocity and acceleration [32]. The position, velocity, and acceleration segments were then combined to form an $n \times 3$ matrix while the segmented torque was placed in a $n \times 1$ vector to satisfy the form of Eq. (8) where y is the $n \times 1$ vector of segmented torques, C is the $n \times 3$ regressor matrix of positions, velocities, and accelerations, and x is the 3×1 vector of unidentified impedance parameters. Least-squares system identification was used to calculate the values of the 3×1 vector, x , where the values of x correspond to the values K, B , and J , respectively. These values are used to fit a second-order model of impedance according to Eq. (1)

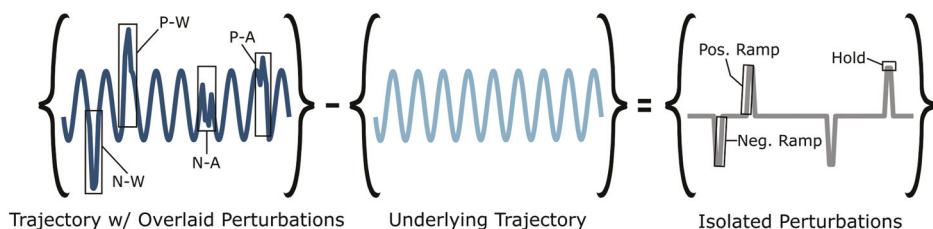


Fig. 4 Diagram of the perturbation response extraction technique. The response to the reference trajectory (light blue) subtracted from the response to the perturbation-augmented reference trajectory (dark blue) yields the response to the perturbations alone (gray). The experiment featured four types of perturbations: a positive torque perturbation in the same direction as the underlying trajectory (P-W), a negative torque perturbation in the same direction as the underlying trajectory (N-W), a positive torque perturbation in the opposite direction as the underlying trajectory (P-A), and a negative torque perturbation in the opposite direction as the underlying trajectory (N-A). Each perturbation had a 75 ms ramp up from zero to seven Nm (pos. ramp), followed by a constant seven Nm output for 100 ms (hold), and concluded with a 75 ms ramp down from seven to zero Nm (neg. ramp).

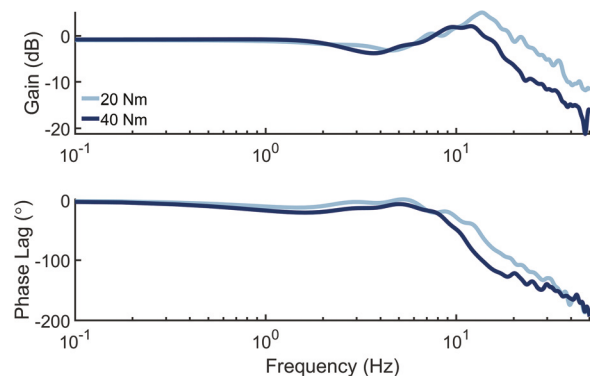


Fig. 5 Plot of the actuator's torque bandwidth at 20 and 40 N·m. Bandwidth was determined by measuring the system's torque response to a filtered Gaussian white noise (FGWN) signal with a cutoff frequency of 30 Hz.

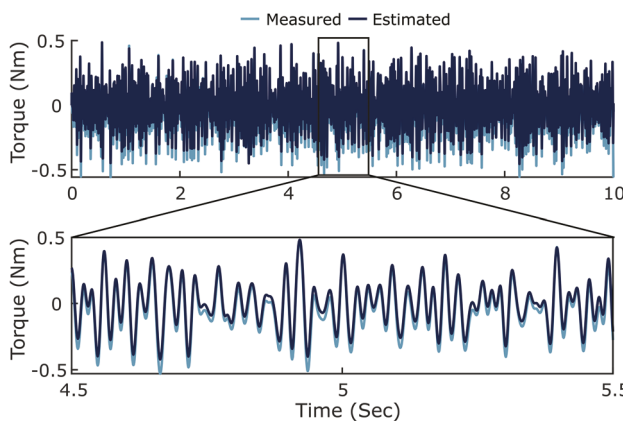


Fig. 6 Plot of estimated torque using mean estimated impedance values and filtered measured torque for a representative trial. VAF captures how similar the estimated signal is to the original filtered signal. The top section shows the full signal and the bottom section shows the boxed in portion of the top plot; a one second window.

$$y = Cx \quad (8)$$

We conducted seven trials for each reference trajectory, during which the output shaft position and torque from were measured at a sample rate of 900 Hz. Accuracy of stiffness and inertia estimates were quantified using percent error to compare model estimated values to the known spring-inertia values.

2.5 Statistical Analysis of Impedance Estimates. Analysis of variance was performed on the estimates of stiffness, damping, and inertia to assess the significance of experimental factors on the analysis. A general linear model was used to evaluate

stiffness, damping, and inertia for under all conditions. For the analysis of stiffness and inertia, the perturbation direction (i.e., if the perturbation was in the same or opposite direction of the underlying trajectory), the perturbation type (i.e., whether the perturbation was a positive or negative torque perturbation), the underlying trajectory frequency (0.8, 1.4, 1.7, or 2.0 Hz), and parameter type (k_1 or k_2 for stiffness and I_1 or I_2 for inertia) were treated as fixed factors. For the analysis of damping, parameter type was not considered as a factor. Each of the three impedance parameters were considered as a dependent variable, and a separate analysis was completed for each. The length of the vector for each response variable was 16,000 elements, which stemmed from the multiplication of the number of bootstrap iterations at each timing point (100), the number of timing points (8), the number of cases (4), and the number of trajectories (5). A Bonferroni correction was used for all posthoc comparisons, and the significance level for all tests was set at $\alpha = 0.05$. VAF was calculated for torque estimated from impedance parameters and the measured torque signal.

3 Results

3.1 Characterization of Exoskeleton Bandwidth and Intrinsic Impedance. The system bandwidth was found to be 26.8 Hz for the 20 Nm reference input and 17.2 Hz for the 40 Nm reference input (Fig. 5). The average intrinsic stiffness, damping, and inertial components of the exoskeleton were found to be 0.5 ± 0.2 Nm/rad, 0.2 ± 0.0 Nms/rad, and 9.1 ± 0.2 kgcm², respectively. The model fit showed an average VAF of $92.5 \pm 4.7\%$ across all trials (Fig. 6).

3.2 Computation of External Inertia and Spring Stiffness Values. The average, ground-truth measurements for each component of the three part inertia are shown in Table 1. The inertia with the aluminum center bar (I_1) was 364.0 ± 0.5 kgcm², while the inertia with the steel center piece (I_2) was 700.0 ± 2.0 kgcm². The weights used to calculate stiffness for k_1 were $W_1 = 182.7$ N and $W_2 = 356$ N. The weights used for k_2 had magnitudes of $W_1 = 184$ N and $W_2 = 356$ N. Final spring calculations showed the stiffness of k_1 to be 168.0 ± 14.3 Nm/rad and k_2 to be 273.0 ± 13.9 N·m/rad.

3.3 Dynamic Estimation of Mechanical Impedance. Stiffness estimates were more accurate than inertia values (Fig. 7). On average, errors for the stiffness estimates were $-2.9 \pm 3.8\%$ for k_1 and $-2.5 \pm 5.8\%$ for k_2 . Average errors for the inertia estimates were $-16.3 \pm 9.2\%$ for I_1 and $-13.0 \pm 6.3\%$ for I_2 . The spring and inertia with greater magnitudes (i.e., k_2 and I_2) were estimated more accurately than their smaller counterparts (i.e., k_1 and I_1), with the most accurate average estimate stemming from k_2 following trajectory D (Table 2). The mean damping value across all trials was 0.3 ± 0.4 Nms/rad.

3.4 Statistical Analysis of Stiffness and Inertia Estimates. The VAF values for all case-trajectory combinations were above

Table 1 Average dimensions, centroid distance to axis of rotation (AOR), and mass for each component of the three bar inertia

Component	Length (cm)	Width (cm)	Height (cm)	Centroid distance to AOR (cm)	Mass (kg)
Top bar	1.0 ± 0.0	25.0 ± 0.0	2.0 ± 0.0	21.5 ± 0.1	0.1 ± 0.0
Bottom bar	1.0 ± 0.0	24.9 ± 0.0	2.0 ± 0.0	21.5 ± 0.1	0.1 ± 0.0
Middle aluminum Bar	1.8 ± 0.0	12.0 ± 0.0	5.0 ± 0.0	27.9 ± 0.0	0.3 ± 0.0
Middle steel bar	1.8 ± 0.0	9.4 ± 0.0	5.0 ± 0.0	29.3 ± 0.0	0.7 ± 0.0

All distances and masses were determined through caliper and scale measurement, respectively. Measurements were taken three times and then averaged to produce the results displayed.

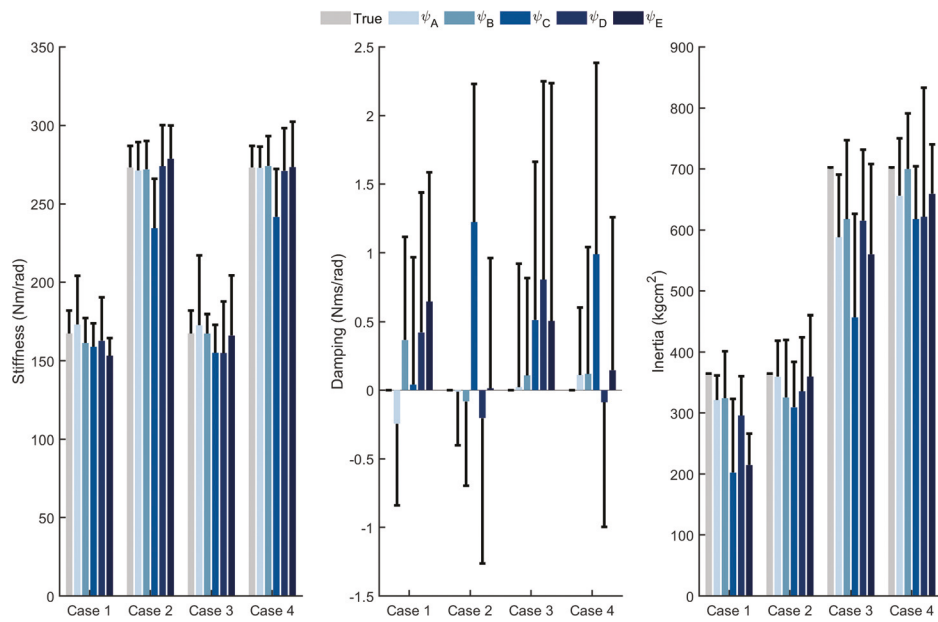


Fig. 7 Plot of estimated torque using mean estimated impedance values and filtered measured torque for a representative trial. VAF captures how similar the estimated signal is to the original filtered signal. The top section shows the full signal and the bottom section shows the boxed in portion of the top plot; a one second window.

99% showing strong agreement between the estimated parameters and the measured data. The analysis of variance results show that almost all of the factors in all linear models had a statistically significant effect. The exception to this would be parameter type for the linear model of stiffness ($p = 0.3$, $F_{1,15999} = 1.1$). The posthoc analysis on the effect of frequency showed different levels of stratification for each impedance estimate. Stiffness estimates with ψ_c as the underlying trajectory were significantly different from all other estimates. Damping estimates were sectioned into three distinct groups: estimates at 0.8 and 1.4 Hz, 1.7 Hz, and 2.0 Hz. Finally, the posthoc comparison of inertia showed that each frequency yielded statistically different estimates from all other frequencies, with the frequencies having the closest relationship being 0.8 and 1.4 Hz.

4 Discussion

The objective of this study was to investigate the system identification capabilities of a torque-controlled knee exoskeleton for future applications of characterizing human knee mechanical impedance. Our methods included characterization of system torque bandwidth and intrinsic impedance, as well as implementation of perturbation-based system identification techniques to estimate the mechanical impedance of external mass-spring systems. We chose system parameters that could best emulate the characteristics of human locomotion in a bench top setting. The system's minimum

bandwidth was 17.6 Hz. The bandwidth is not expected to affect high-fidelity tracking of our perturbation trajectories, which have 99% of their signal power below 9 Hz. The intrinsic impedance was found to be low in comparison to the tested external mechanical systems. Estimated external impedance results were comparable to values seen in literature; stiffness estimate errors were under 3%, and inertia estimate errors ranged from ~13 to 16%.

4.1 Stiffness and Inertia Estimates. The accuracy of the stiffness and inertia estimates from our approach are similar to or better than previous works. The average stiffness errors for the two tested springs (2.5% and 2.9%) were lower than the reported average stiffness errors of other systems designed for determining joint mechanical impedance (approximately 5% [4] and 15% for 13 of 18 trials [22] in the lower limb and 9% in the upper limb [33]). The average inertia estimate errors from our system (13.0% and 16.3%) were comparable to those reported by Tucker et al. for the lower limb (15% for 16 of 18 trials [22]) and slightly higher than the maximum error of 11% seen in the upper limb [33].

For most of the tested trajectories, we noted better estimates of stiffness and inertia at higher values of these parameters. The exceptions to this trend were the inertia estimates for Trajectory A and stiffness estimates for Trajectory C. We attribute these trends to constant torque measurement error, whose effects become

Table 2 Average percent error and standard deviation of stiffness (K) and inertia (I) estimates for each trajectory

K table	Trajectory A	Trajectory B	Trajectory C	Trajectory D	Trajectory E
K_1	3.2 ± 0.2	-1.9 ± 2.5	-6.2 ± 1.6	-5.2 ± 3.3	-4.7 ± 5.4
K_2	-0.4 ± 0.4	-0.1 ± 0.6	-12.8 ± 1.9	0.3 ± 0.8	1.1 ± 1.4
I table	Trajectory A	Trajectory B	Trajectory C	Trajectory D	Trajectory E
I_1	-6.5 ± 7.4	-10.7 ± 0.2	-29.7 ± 20.7	-13.3 ± 7.7	-21.1 ± 28.1
I_2	-11.1 ± 6.8	-5.9 ± 8.2	-23.2 ± 16.3	-11.6 ± 0.7	-12.9 ± 10.0

Average stiffness percent error estimates were determined through averaging stiffness results from cases 1 and 3 for K_1 and cases 2 and 4 for K_2 . Average inertial percent error estimates were obtained after averaging results from cases 1 and 2 for I_1 and cases 3 and 4 for I_2 .

increasingly mitigated as externally applied torque increases (i.e., larger stiffness and inertia values). Our stiffness estimates were more accurate when compared to estimates of inertia. Stiffness estimates had both lower maximum and minimum errors, when compared to inertia estimates, as well as reduced standard deviations. Segmenting measured torque according to the relative contributions of each component (Eq. (1)) offers insight into our results; the $k\theta$ component of torque is greater than the $J\dot{\theta}$ component. Alternatively, a larger error in estimating the inertial torques could be attributed to the numerical method used to determined velocity and acceleration, which tends to lose fidelity with higher order derivatives.

4.2 Statistical Analysis. Statistical analysis shows that the parameter estimates accurately model measured torque behavior. VAF was high in all cases ($>99\%$), which is expected, given the second order dynamics of mass-spring systems. Our VAF measurements compare favorably to other joint impedance measurement devices. Rouse et al. reported an average VAF of 99.1% during the validation of their device while Tucker et al. reported VAF's ranging from 87.2% to 99.9% during their characterization process. High model fit during these ideal conditions is important because we would expect model fit to worsen with human subject testing. The device used by Rouse and Shorter to measure dynamic ankle impedance during stance saw, its average VAF results drop from 99.1% to $92 \pm 6.3\%$ and $90 \pm 7.7\%$, respectively, during human testing [4,24]. Lee saw an average VAF of 85.7 ± 4.5 during their characterization of ankle impedance during the swing phase of walking [23]. Having a near perfect model fit under idealized conditions increases confidence in this device's ability to be deployed in the field to estimate knee joint impedance during walking.

4.3 Experimental Implications. The results revealed that the frequency of the applied reference trajectory affects the quality of the resulting impedance estimate. Trajectories A, B, and D had frequencies ranging from 0.8 to 1.4 Hz, which fall under slow walking or pathological gait [4,23,29,30]. Trajectories C and E had frequencies ranging from 1.7 to 2.0 Hz, which is more similar to able-bodied human gait [27]. We found that impedance estimates from trajectories at lower frequencies were more accurate, with lower stiffness and inertia estimate errors and damping estimates closer to zero. Performing experiments to measure joint mechanical impedance at gait frequencies lower than those typically seen during able-bodied human gait is not unprecedented; previous work characterizing human joint impedance during locomotion collected data at gait frequencies lower than the frequency of able-bodied human gait [4,23,24].

The form that the results of how knee mechanical impedance varies during walking will have is unclear; however, we can look to literature to infer how our validation results will translate to human experiments and if the error of these results is sufficient to produce estimates during human experimentation that can be trusted. We know that measurements of stiffness obtained during locomotion are lower than what postural studies would predict. Thus, we postulate that case 2 results may emulate human testing conditions well, since it includes the lowest stiffness tested and the full inertia of the leg [13]. For these conditions tested at gait speeds at or below 1.4 Hz, we would expect stiffness errors of below 1% and a max inertia error of $\sim 10\%$. Our percent errors for stiffness and inertia estimates as well as the VAF associated with these terms is equal to or better than other state of the art joint mechanical impedance measurement tools. However, what is unknown is if the error associated with our measurements is small enough to permit the use of our results in other domains, such as robotic control. Literature may provide us an insight into this question. Azocar et al. showed that humans in a seated position can, at best, perceive stiffness changes of 11.6% and 13.4% at the knee and ankle, respectively. [34]. Our stiffness error measurements of 3% are well under those numbers and lead us to believe

that our stiffness estimates will not only be accurate, but can also be practically applied to robotic control of wearable devices like prosthetic limbs, due to our errors being below the threshold of human perception.

4.4 Limitations. Although experimental methods and device encumbrances did affect our results, this device shows promise for obtaining estimates of mechanical impedance using the proposed methods. The bench top setup did not include an explicit damper, and validation of the system identification capabilities of the device was limited to measures of stiffness and inertia. We did, however, report a damping estimate in our results. We hypothesized that our estimates of damping should reflect the lack of an explicit damper in the system, resulting in a mean damping estimate close to zero with some noise. The average damping estimate was close to zero, at 0.3 ± 0.4 Nms/rad, which was an encouraging result, as it aligned with our initial expectations. While we cannot make any definitive claims on the damping estimation abilities of our system, we interpret these data to reflect positively on the potential of our approach to measure human knee damping in future studies.

Another limitation to consider is that impedance estimates tended to fall below the true values. Inertia values revealed a notable skew toward underestimation; inertia estimates for 100% of tested trajectories and case-trajectory combinations were underestimates of the true value. Examining stiffness estimates by trajectory revealed that 80% of the estimates fell below the true value. Examining stiffness estimates by case and trajectory, however, revealed that 43% of the underestimates were within 1% of their true value. We conclude that while inertia estimates were skewed toward underestimation, stiffness estimates were not as strongly skewed in a single direction. Underestimation could be attributed to inherent variation in the torque applied by the exoskeleton; in a prior study characterizing the exoskeleton, output torque varied by up to $\sim 10\%$. This may arise from inaccuracies in the equation describing the series leaf spring stiffness or from nonlinearities of the leaf spring that are not captured by the linear model implemented in our approach. Overall, the accuracy of impedance estimates reported here, particularly for stiffness and damping, indicates that this issue can be overcome.

4.5 Future Directions. Knowledge of knee mechanical impedance can be used to further rehabilitative practices, prosthetic design, and robotic control. By determining knee impedance values for physically impaired and able-bodied individuals alike, we can use impedance as a metric for rehabilitation. Knowing how an individual's joint impedance varies after a medical intervention or rehabilitative protocol can be a tool for benchmarking patient progress. Knowledge of how mechanical impedance varies can also be used for intelligent design of passive or quasi-passive prosthetic devices. Previous Work shows how biological data can be used to design quasi-passive devices that perform comparably to their powered counterparts but show notable savings in weight and complexity [35,36]. Using a similar approach with knee impedance data could prove beneficial in informing design requirements for the next generation of knee prostheses. Finally, task-based knowledge of knee mechanical impedance provides opportunities for new control methodologies. Using our approach, we can definitively replicate the mechanical impedance of human joints, accurately and simultaneously replicating knee torque, angle, and mechanical impedance.

5 Conclusion

In this work, we validated the system identification capabilities of a torque-controllable knee exoskeleton and proposed a perturbation paradigm for the identification of the impedance known mass-spring systems with the intention of extending this work to estimate the mechanical impedance of the human knee during

locomotion. Our proposed methods yielded stiffness estimate errors of ~ 2 to 3% damping values centered around zero and dominated by variability and inertia estimate errors ranging from ~ 13 to 16%. We also learned that our analysis techniques tend to underestimate impedance parameters and that experimental factors such as the frequency of the underlying trajectory and type of perturbation applied by the exoskeleton have an effect on the efficacy of the results of our approach. From the conclusions, we believe that this tool can be utilized to characterize human knee joint mechanical impedance during locomotion in future studies.

Funding Data

- NSF CAREER (Award No. 1846969; Funder ID: 10.13039/100000001).
- NSF Graduate Research Fellowship (Award No. DGE 1256260; Funder ID: 10.13039/100000001).

References

- 1 Neptune, R. R., Zajac, F. E., and Kautz, S. A., 2004, "Muscle Force Redistributions Segmental Power for Body Progression During Walking," *Gait Posture*, **19**(2), pp. 194–205.
- 2 Winter, D. A., 1983, "Energy Generation and Absorption at the Ankle and Knee During Fast, Natural, and Slow Cadences," *Clin. Orthop. Relat. Res.*, **175**, pp. 147–154.
- 3 Kearney, R. E., and Hunter, I. W., 1990, "System Identification of Human Joint Impedance," *J. Am. Soc. Inf. Sci.*, **18**, pp. 55–87.
- 4 Rouse, E. J., Hargrove, L. J., Perreault, E. J., and Kuiken, T. A., 2014, "Estimation of Human Ankle Impedance During the Stance Phase of Walking," *IEEE Trans. Neural Syst. Rehabil. Eng.*, **22**(4), pp. 870–878.
- 5 Kuo, A. D., and Donelan, J. M., 2010, "Dynamic Principles of Gait and Their Clinical Implications," *Phys. Ther.*, **90**(2), pp. 157–174.
- 6 Burdet, E., Osu, R., Franklin, D. W., Milner, T. E., and Kawato, M., 2001, "The Central Nervous System Stabilizes Unstable Dynamics by Learning Optimal Impedance," *Nature*, **414**(6862), pp. 446–449.
- 7 Hu, X., Ludvig, D., Murray, W. M., and Perreault, E. J., 2017, "Using Feedback Control to Reduce Limb Impedance During Forceful Contractions," *Sci. Rep.*, **7**(1), pp. 1–13.
- 8 Wind, A. M., and Rouse, E. J., 2020, "Neuromotor Regulation of Ankle Stiffness is Comparable to Regulation of Joint Position and Torque at Moderate Levels," *Sci. Rep.*, **10**(1), pp. 1–9.
- 9 Zhang, L. Q., Nuber, G., Butler, J., Bowen, M., and Rymer, W. Z., 1997, "In Vivo Human Knee Joint Dynamic Properties as Functions of Muscle Contraction and Joint Position," *J. Biomech.*, **31**(1), pp. 71–76.
- 10 Lee, H., Ho, P., Rastgaard, M. A., Krebs, H. I., and Hogan, N., 2011, "Multivariable Static Ankle Mechanical Impedance With Relaxed Muscles," *J. Biomech.*, **44**(10), pp. 1901–1908.
- 11 Bennett, D. J., Hollerbach, J. M., Xu, Y., and Hunter, I. W., 1992, "Time-Varying Stiffness of Human Elbow Joint During Cyclic Voluntary Movement," *Exp. Brain Res.*, **88**(2), pp. 433–442.
- 12 Popescu, F., Hidler, J. M., and Rymer, W. Z., 2003, "Elbow Impedance During Goal-Directed Movements," *Exp. Brain Res.*, **152**(1), pp. 17–28.
- 13 Ludvig, D., Plocharski, M., Plocharski, P., and Perreault, E. J., 2017, "Mechanisms Contributing to Reduced Knee Stiffness During Movement," *Exp. Brain Res.*, **235**(10), pp. 2959–2970.
- 14 Pfeifer, S., Vallery, H., Hardegger, M., Riener, R., and Perreault, E. J., 2012, "Model-Based Estimation of Knee Stiffness," *IEEE Trans. Biomed. Eng.*, **59**(9), pp. 2604–2612.
- 15 Pfeifer, S., Riener, R., and Vallery, H., 2014, "Knee Stiffness Estimation in Physiological Gait," *36th Annual International Conference of the IEEE Engineering in Medicine and Biology Society, EMBC*, Aug. 26–30, Chicago, IL, pp. 1607–1610.
- 16 Sartori, M., Maculan, M., Pizzolato, C., Reggiani, M., and Farina, D., 2015, "Modeling and Simulating the Neuromuscular Mechanisms Regulating Ankle and Knee Joint Stiffness During Human Locomotion," *J. Neurophysiol.*, **114**(4), pp. 2509–2527.
- 17 Shamaei, K., Sawicki, G. S., and Dollar, A. M., 2013, "Estimation of Quasi-Stiffness of the Human Knee in the Stance Phase of Walking," *PLoS One*, **8**(3), p. e59993.
- 18 Rouse, E. J., Gregg, R. D., Hargrove, L. J., and Sensinger, J. W., 2013, "The Difference Between Stiffness and Quasi-Stiffness in the Context of Biomechanical Modeling," *IEEE Trans. Biomed. Eng.*, **60**(2), pp. 562–568.
- 19 Temel, M., Rudolph, K. S., and Agrawal, S. K., 2011, "Gait Recovery in Healthy Subjects: Perturbations to the Knee Motion With a Smart Knee Brace," *Adv. Rob.*, **25**(15), pp. 1857–1877.
- 20 Sulzer, J. S., Roiz, R. A., Peshkin, M. A., and Patton, J. L., 2009, "A Highly Backdrivable, Lightweight Knee Actuator for Investigating Gait in Stroke," *IEEE Trans. Rob.*, **25**(3), pp. 539–548.
- 21 Andersen, J. B., and Sinkjaer, T., 2003, "Mobile Ankle and Knee Perturbator," *IEEE Trans. Biomed. Eng.*, **50**(10), pp. 1208–1211.
- 22 Tucker, M. R., Shiota, C., Lamberty, O., Sulzer, J. S., and Gassert, R., 2017, "Design and Characterization of an Exoskeleton for Perturbing the Knee During Gait," *IEEE Trans. Biomed. Eng.*, **64**(10), pp. 2331–2343.
- 23 Lee, H., and Hogan, N., 2015, "Time-Varying Ankle Mechanical Impedance During Human Locomotion," *IEEE Trans. Neural Syst. Rehabil. Eng.*, **23**(5), pp. 755–764.
- 24 Shorter, A. L., and Rouse, E. J., 2018, "Mechanical Impedance of the Ankle During the Terminal Stance Phase of Walking," *IEEE Trans. Neural Syst. Rehabil. Eng.*, **26**(1), pp. 135–143.
- 25 Shepherd, M. K., and Rouse, E. J., 2017, "Design and Validation of a Torque-Controllable Knee Exoskeleton for Sit-to-Stand Assistance," *IEEE/ASME Trans. Mechatronics*, **22**(4), pp. 1695–1704.
- 26 Challis, J. H., Winter, S. L., and Kuperavage, A. J., 2012, "Comparison of Male and Female Lower Limb Segment Inertial Properties," *J. Biomech.*, **45**(15), pp. 2690–2692.
- 27 Pachi, A., and Ji, T., 2005, "Frequency and Velocity of People Walking," *Struct. Eng.*, **84**(3), pp. 36–40.
- 28 Lee, H., Rouse, E. J., and Krebs, H. I., 2016, "Summary of Human Ankle Mechanical Impedance During Walking," *IEEE J. Transl. Eng. Health Med.*, **4**, pp. 1–7.
- 29 Fulk, G., Ludwig, M., Dunning, K., Golden, S., Boyne, P., and West, T., 2011, "Estimating Clinically Important Change in Gait Speed in People With Stroke Undergoing Outpatient Rehabilitation," *J. Neurol. Phys. Ther. JNPT*, **35**(2), pp. 82–89.
- 30 Akosile, C. O., Adegoke, B. O. A., Raji, N. O., Anyanwu, C. C., and Orji, G. C., 2013, "Gait Quality and Physical Functioning of Stroke Survivors With and Without Aphasia," *Hong Kong Physiother. J.*, **31**(1), pp. 25–29.
- 31 Rouse, E. J., Hargrove, L. J., Perreault, E. J., Peshkin, M. A., and Kuiken, T. A., 2013, "Development of a Mechatronic Platform and Validation of Methods for Estimating Ankle Stiffness During the Stance Phase of Walking," *ASME J. Biomed. Eng.*, **135**(8), pp. 1–8.
- 32 Scheid, F., 1988, *Schaum's Outline of Theory and Problems of Numerical Analysis*, McGraw-Hill, New York.
- 33 Acosta, A. M., Kirsch, R. F., and Perreault, E. J., 2000, "A Robotic Manipulator for the Characterization of Two-Dimensional Dynamic Stiffness Using Stochastic Displacement Perturbations," *J. Neurosci. Methods*, **102**(2), pp. 177–186.
- 34 Azocar, A. F., and Rouse, E. J., 2017, "Stiffness Perception During Active Ankle and Knee Movement," *IEEE Trans. Biomed. Eng.*, **64**(12), pp. 2949–2956.
- 35 Shepherd, M. K., and Rouse, E. J., 2017, "The VSPA Foot: A Quasi-Passive Ankle-Foot Prosthesis With Continuously Variable Stiffness," *IEEE Trans. Neural Syst. Rehabil. Eng.*, **25**(12), pp. 2375–2386.
- 36 Glanzer, E. M., and Adamczyk, P. G., 2018, "Design and Validation of a Semi-Active Variable Stiffness Foot Prosthesis," *IEEE Trans. Neural Syst. Rehabil. Eng.*, **26**(12), pp. 2351–2359.